distributions rather well, whereas only the (d,p) $f_{5/2}$ angular distributions are fitted by the calculations, and these require a 5 F cutoff radius. In Fig. 2 the shapes of measured $f_{5/2}$ transitions from the (d,p) and (p,d) reactions are compared with those from $f_{7/2}$ transitions.

From Figs. 1 and 2 it is apparent that the forward angle J dependence is significantly less in the present data than in the ^{56}Fe$(p,d)^{55}$Fe reaction. This may simply reflect the difference in the Q values between the studied (d,p) and (p,d) reactions. However, if the Q dependence is predicted correctly by the DWBA calculations, these data strongly support the explanation of the forward angle J dependence in terms of configuration mixing effects since the DWBA predictions for the nonconfiguration mixed $f_{7/2}$ transitions closely agree with experiment while the $f_{5/2}$ data are only fitted where the transferred neutron should be well described by a single-particle wave function (though one should note that a 5 F cutoff radius is needed to fit the $f_{5/2}$ data, while the $f_{7/2}$ data is fitted without a cutoff). It is also apparent from the data that there is a residual J dependence which is possibly a consequence of the D state of the deuteron as has been suggested by Johnson and Santos.[8] Since the calculations by Johnson and Santos[8] were not able to reproduce the full J dependence observed in the $l=3$ (p,d) reactions, it will be of particular interest to see whether their method of calculation can reproduce the present data, in which configuration mixing effects are of lesser importance.

The authors thank Dr. D. A. Bromley for helpful discussions concerning this manuscript, and Dr. B. Zeidman for his kind loan of the ^{48}Ti foil.

PHYSICAL REVIEW VOLUME 170, NUMBER 4 20 JUNE 1968

Continuum Nuclear Structure of O^{16} in the Eigenchannel Reaction Theory*

H. G. Wahsweiler and Walter Greiner
Institut fur Theoretische Physik der Universitat Frankfurt, Frankfurt Main, Germany

and

Michael Danos
National Bureal of Standards, Washington, D. C. 20234

(Received 29 November 1967)

The total particle-particle S^J matrix of O^{16} for spin $J=1^-$ and excitation energies between 15 and 27 MeV has been calculated in the eigenchannel reaction theory for several parameters of the Saxon-Woods potential and the two-body force. The many-body problem has been treated in the 1-particle–1-hole approximation. The photon channels have been included by perturbation theory. Surprisingly, the most important structure of the experimental cross sections is reproduced quite well in this simple approximation.

1. INTRODUCTION

THE proper theoretical treatment of the nuclear continuum has been one of the important challenges to nuclear theorists in recent years. Attempts have been made by various groups[1–11] to solve the problem at least for that case where only one nucleon is in the continuum, i.e., below the two-nucleon threshold. Since a nuclear reaction can be described only as a particular continuum state of the nuclear-system target plus projectile, it is clear that unambiguous statements about the target structure can be made only by a correct treatment of the continuum problem.

The calculations in the present paper are performed by applying the methods of the eigenchannel theory. The formal aspects of this theory have been presented earlier.[7,12] In this paper, first, we supplement the earlier treatment[7] by giving the details necessary for an actual calculation and, second, we discuss the results obtained in a computation of the 1^- compound system O^{16} in the 1-particle–1-hole approximation. Thus, our calculation encompasses the $N^{15}+p$ and the $O^{15}+n$ reactions as

* This work has been supported by the Deutsche Forschungsgemeinschaft with a contract for studies in Nuclear Structure.

[1] R. H. Lemmer and C. M. Shakin, Ann. Phys. (N. Y.) **27**, 13 (1964).
[2] W. M. MacDonald, Nucl. Phys. **54**, 393 (1964); **56**, 636 (1964).
[3] C. Bloch and V. Gillet, Phys. Letters **16**, 62 (1965); **18**, 58 (1965).
[4] J. Raynal, M. A. Melkanoff, and T. Sawada, Saclay Report, 1967 (unpublished).
[5] H. A. Weidenmüller, Nucl. Phys. **75**, 189 (1966).
[6] B. Buck and A. D. Hill, Nucl. Phys. **A95**, 271 (1967).
[7] M. Danos and W. Greiner, Phys. Rev. **146**, 708 (1966).
[8] H. G. Wahsweiler, M. Danos, and W. Greiner, Phys. Rev. Letters **17**, 395 (1966).
[9] H. G. Wahsweiler, M. Danos, and W. Greiner, Phys. Letters **23**, 257 (1966).
[10] V. Gillet, M. A. Melkanoff, and J. Raynal, Nucl. Phys. **A97**, 631 (1967).
[11] M. Marangoni and A. M. Saruis, Phys. Letters **24B**, 218 (1967).
[12] M. Danos and W. Greiner, Z. Physik **202**, 125 (1967).

well as the reactions induced by photons incident on O^{16}. Our results indicate that the main features of the photon-absorption process can be reproduced by an appropriate choice of the nuclear parameters.

The basic idea of the eigenchannel theory is to construct, at a given excitation energy of the A-particle system (i.e., the system target plus projectile), a complete set of scattering states, the eigenchanngel states, which diagonalize simultaneously the nuclear Hamiltonian and the S matrix. If at that energy there are N open "experimental" channels, then the S matrix is an $N\times N$ matrix and there are N eigenchannels. Because of unitarity the eigenvalues of the S matrix can be written in terms of real phases $\delta^{(\nu)}$ as $e^{2i\delta^{(\nu)}}$. If the channels of the actual many-channel problem are decoupled the system is reduced to the simple case of the scattering of particles by a real potential. Then the eigenphases $\delta^{(\nu)}$ go over into the potential-scattering phases, and the eigenchannels become indentical with the experimental channels. In general, the eigenchannels are linear superpositions of the experimental channels such that there are standing waves in all experiment channels which all have a common phase shift, the eigenphase. Denoting the amplitudes of the experimental channels c in a given eigenchannel ν by $V_c^{(\nu)}$, the S matrix is given by

$$S_{cc'}=\sum_{\nu} V_c^{(\nu)} e^{2i\delta^{(\nu)}} V_{c'}^{(\nu)}.$$

Thus it can be easily computed once the eigenchannels are known. Therefore the central point is the problem of finding such an eigenstate of the Hamiltonian which is an eigenchannel rather than a superposition of eigenchannels. This problem was solved by employing a search which leads directly to the eigenchannels.

In the present paper, as in the other calculations, the proton and the neutron states were treated independently since the Coulomb energy is much too large to be neglected; and the center-of-mass (c.m.) motion has not been properly taken care of. Therefore, the results will be uncertain to some extent because the spurious states are contained in the nuclear wave function. The accuracy of the results is also affected by the size of the set of basis states actually used in the computations and by the magnitude of the matching radius. These points will be discussed below in detail.

This calculation is, strictly speaking, incomplete in that it neglects the more complicated reactions involving the emission of α particles, of deuterons, or of an unbound proton-neutron pair.[12] To that end one would have to include many-particle–many-hole states in the nuclear wave function. These components would also lead to fine structure in the cross sections.[10] Such a calculation is in preparation.

The photon channels are treated, as usual, by perturbation methods. The electromagnetic interaction induces a transition between the ground state and a general scattering state, This is permissible since, in contrast to incoming particles, photons interact with the nuclear system only weakly. A direct inclusion of photon channels into the S matrix thus is totally unnecessary.

The paper is organized as follows. In Sec. 2 the definitions of all relevant quantities are given and the expressions for the particle cross sections in terms of the eigenchannel parameters are written down. It turns out that the form of these expressions is completely analogous to the form of the scattering cross sections for potential scattering. The photon absorption process is discussed in Sec. 3. Some care has to be taken in the evaluation of the density of the final states because, in general, the final state contains more than one open channel and the momenta of the outgoing particles in the different channels are, in general, different. The procedures of the actual calculations and the choice of the model parameters are described in detail in Sec. 4. This section also contains the discussion of the different parameters which affect the accuracy of the calculations and a description of the tests which were performed to check the degree of validity of the results. Finally, the results are discussed and compared with experiment in Sec. 5.

2. PARTICLE-PARTICLE REACTION CROSS SECTIONS

In this section we give the expressions of angular distributions, partial and total cross sections for particle-particle reactions in terms of the eigenphases and the eigenvectors of the S matrix. We closely follow the treatment of Ref. 13.

Let us first recapitulate the case of elastic scattering of a single spinless particle by a central force (potential scattering). There the particle cross section $d\sigma$ is

$$d\sigma=|f(\theta)|^2 d\Omega, \tag{2.1}$$

with the following scattering amplitude:

$$f(\theta)=i\pi^{1/2}\lambda\sum_{l=0}^{\infty}(2l+1)^{1/2}(1-e^{2i\delta_l})Y_{l0}(\theta). \tag{2.2}$$

δ_l are the scattering phases which here simply are the eigenphases of the one-dimensional S matrices, one for each angular momentum l, and λ denotes the wavelength of the scattering particle. By applying the addition theorem for spherical harmonics, one obtains

$$d\sigma/d\Omega=\lambda^2\sum_{L=0}^{\infty} B_L P_L(\cos\theta), \tag{2.3}$$

with

$$B_L=\sum_{l=0}^{\infty}\sum_{l'=|l-L|}^{l+L}(2l+1)(2l'+1)\times[(ll'00|L0)]^2\sin\delta_l\sin\delta_{l'}\cos(\delta_l-\delta_{l'}). \tag{2.4}$$

[13] J. M. Blatt and L. C. Biedenharn, Rev. Mod. Phys. **24**, 258 (1952).

Then the integrated cross section is given by

$$\sigma_0=4\pi\lambda^2 B_0. \tag{2.5}$$

The cross sections thus can be readily calculated if the eigenphases (scattering phases) of the S matrices are known. In the general case of interacting channels, the cross section is given by an analogous expression which, besides the eigenphases, also contains the amplitudes $V_c^{(\nu)}$. We now turn to the description of the general case.

A. Nuclear Wave Function

We begin by considering the region $r\leq a$ of the ordinary space where the influence of the nuclear interactions is non-negligible. There we describe the A-particle system by an expansion into particle-hole configurations. As stated in the Introduction, we shall consider only the 1-particle–1-hole terms. Since the space $r\leq a$ is finite, we have to deal only with discrete states. Thus the 1-particle–1-hole basis functions can be put into the form

$$\begin{aligned}|n_a n_A; j_a j_A m_\tau^A; JM\rangle\rangle=&\sum_m(-)^{j_A-m}\\ &\times(j_a j_A M+m\ -m|JM)|(l_a s_a)j_a M+m\rangle^*\\ &\times|(l_A s_A)j_A m\rangle r_a^{-1}u_{n_a l_a j_a}(r_a)\\ &\times r_A^{-1}u_{n_A l_A j_A}(r_A)|\tau_a m_\tau^A\rangle^*|\tau_A m_\tau^A\rangle.\end{aligned} \tag{2.6}$$

Our nomenclature corresponds to that used by Gillet.[14,15] Quantum numbers with upper-case subscripts or superscripts refer to particles and those with lower-case subscripts or superscripts refer to holes. Since the proton and neutron radial wave functions may differ strongly in the continuum, we do not use the isospin formalism, but treat neutrons and protons separately. The kets in (2.6) containing τ characterize the charge of the nucleon. n is the radial quantum number. This completes the definition of the set of basis functions in which the Hamiltonian will be diagonalized.

In deriving the cross-section formulas (see Sec. 2 C below), we shall need a wave function in which the N orthogonal eigenchannel functions have been superposed in such a way that they asymptotically represent an incoming plane wave plus outgoing spherical waves. For well-known reasons it is advantageous to do this in the channel spin representation. Thus we introduce the channel spin s by coupling the spin s_A of the scattering particle to the nuclear spin j_a of the $(A-1)$ particle system:

$$\begin{aligned}\Psi_{j_a s_A}{}^{s\mu}=&\sum_\nu(-)^{1/2-\nu}(j_a s_A\mu+\nu\ -\nu|s\mu)\\ &\times|j_a\mu+\nu\rangle^*|s_A\nu\rangle.\end{aligned} \tag{2.7}$$

The channel spin then can be coupled to the angular momentum l_A of the particle to give the spin J of the compound system

$$\mathcal{Y}_{Jl_A s}{}^M=\sum_\mu(l_A sM-\mu\mu|JM)\Psi_{j_a s_A}{}^{s\mu}Y_{l_A M-\mu}(\Omega_A). \tag{2.8}$$

Finally, we define the internal function of the $(A-1)$ system:

$$\varphi_\alpha=r_a^{-1}u_{n_a l_a j_a}(r_a)|\tau_a m_\tau^A\rangle^*|\tau_A m_\tau^A\rangle. \tag{2.9}$$

Here α denotes the set of quantum numbers $n_a l_a j_a m_\tau^A$. Now the basis functions (2.6) can be rewritten in the form

$$\begin{aligned}&|n_a n_A; j_a j_A m_\tau^A; JM\rangle\rangle\\ &\quad=\sum_s K_{\alpha s l_A j_A}{}^J\mathcal{Y}_{Jl_A s}{}^M\varphi_\alpha r_A^{-1}u_{n_A l_A j_A}(r_A),\end{aligned} \tag{2.10}$$

where

$$\begin{aligned}K_{\alpha s l j}{}^J=(-)^{s+j_a+j_A+l_A}&[(2j_A+1)(2s+1)]^{1/2}\\ &\times\begin{Bmatrix}s & j_a & \frac{1}{2}\\ j_A & l_A & J\end{Bmatrix}.\end{aligned} \tag{2.11}$$

The recoupling coefficients K fulfil the orthogonality relations

$$\begin{aligned}\sum_s K_{\alpha s l j}{}^J K_{\alpha s l j'}{}^J&=\delta_{jj'},\\ \sum_j K_{\alpha s l j}{}^J K_{\alpha s' l j}{}^J&=\delta_{ss'}.\end{aligned} \tag{2.12}$$

However, we will not define the "experimental channel" c in the channel spin representation, but we shall characterize it by the quantum numbers α, l_A, and j_A. The "channel function" $\tilde{\psi}_c$ is introduced by

$$|n_a n_A; j_a j_A m_\tau^A; JM\rangle\rangle=u_{n_A c}(r_A)\tilde{\psi}_c, \tag{2.13}$$

where u denotes the same radial function as in (2.10).

B. Eigenchannels of the S Matrix

Now we turn to the asymptotic region $r>a$. For the convenience of the reader, we will collect a few relations concerning the eigenchannels and the S matrix which will be needed later. They all result from the unitarity of the S matrix.

The νth eigenchannel $V_{\alpha l_A j_A}{}^{J,\nu}$ of the S matrix S^J for a compound state of angular momentum J is defined by the eigenvalue equation

$$S^J V^{J,\nu}=\epsilon_\nu{}^J V^{J,\nu}, \tag{2.14}$$

where $\epsilon_\nu{}^J=e^{2i\delta_J{}^{(\nu)}}$ and the real quantity $\delta_J{}^{(\nu)}$ is the νth eigenphase of the S^J matrix. There are as many eigenphases as there are open channels and the $V_c{}^{J,\nu}$ form a quadratic matrix. Equation (2.14) is, explicitly,

$$\begin{aligned}\sum_{\alpha' l_A' j_A'}&S_{\alpha' l_A' j_A';\alpha l_A j_A}{}^J V_{\alpha' l_A' j_A'}{}^{J,\nu}\\ &=e^{2i\delta_J{}^{(\nu)}}V_{\alpha l_A j_A}{}^{J,\nu}.\end{aligned} \tag{2.15}$$

[14] V. Gillet, thesis, Saclay, 1962 (unpublished).
[15] V. Gillet and N. Vinh Mau, Nucl. Phys. 54, 321 (1964).

The coefficients $V_c^{J,\nu}$ are orthogonal and can be normalized to unity. They can be assumed to be real. In terms of the $V^{J,\nu}$'s and $\delta^{(\nu)}$'s the S matrix is given by

$$S_{\alpha' l_A' j_A';\alpha l_A j_A}{}^J=\sum_\nu V_{\alpha l_A j_A}{}^{J,\nu} e^{2i\delta_J{}^{(\nu)}} V_{\alpha' l_A' j_A'}{}^{J,\nu}. \quad (2.16)$$

In the channel spin representation $\{\alpha s l_A\}$, the S matrix is given by

$$\tilde{S}_{\alpha' s' l_A';\alpha s l_A}{}^J=\sum_{jj'} K_{\alpha s l_A j}{}^J S_{\alpha' l_A' j';\alpha l_A j}{}^J K_{\alpha' s' l_A' j'}{}^J. \quad (2.17)$$

The recoupling coefficients K are defined in (2.11). In accordance with the definition (2.14), the correctly normalized νth eigenchannel wave function in the asymptotic region is given by

$$\Psi^{J,\nu}=\sum_c \tfrac{1}{2} i v_c^{-1/2} V_c{}^{J,\nu}[e^{-i\delta_J{}^{(\nu)}} I_c - e^{i\delta_J{}^{(\nu)}} O_c]\tilde{\psi}_c, \quad (2.18)$$

where $\tilde{\psi}_c$ is the channel function of channel c introduced in (2.13) and v_c denotes the relative velocity of the particle in this channel. The ingoing and outgoing radial functions I_c and O_c are defined by[16]

$$I_c{}^*=O_c=[G_l(k_c r)+iF_l(k_c r)]e^{-i\omega_c} \rightarrow \exp[i(k_c r-\tfrac{1}{2}l\pi-\eta_c \ln 2k_c r)]. \quad (2.19)$$

Here, F_l and G_l are, respectively, the regular and the irregular solution of the radial differential equation, i.e., they are the Coulomb functions in the case of protons and the spherical Bessel and Neumann functions multiplied by $k_c r$ for neutrons. The Coulomb parameter η_c and the phase ω_c are given by

$$\eta_c=Ze^2/\hbar v_c, \quad \omega_c=\sum_{n=1}^{l} \arctan(\eta_c/n). \quad (2.20)$$

Because of (2.19) the asymptotic eigenchannel function (2.18) can be brought into the form

$$\Psi^{J,\nu}=\sum_{\alpha l_A j_A} v_\alpha{}^{-1/2} V_{\alpha l_A j_A}{}^{J,\nu}\{G_{l_A}(k_\alpha r)\sin(\delta_J{}^{(\nu)}-\omega_{\alpha l_A}) +F_{l_A}(k_\alpha r)\cos(\delta_J{}^{(\nu)}-\omega_{\alpha l_A})\}\tilde{\psi}_{\alpha l_A j_A}. \quad (2.21)$$

The radial parts occurring in (2.21) are real and the eigenchannel functions are standing waves in all experimental channels. They thus resemble a superposition of single-particle radial functions for a real potential. The amplitudes $V_c^{J,\nu}$ can now be determined by equating in the asymptotic region the form (2.21) of the nuclear wave function to that obtained by the diagonalization of the nuclear Hamiltonian in the basis set (2.6). Let us write such a state as

$$\Psi^{J,\nu}=\sum_{\alpha n_A l_A j_A} A_{\alpha n_A l_A j_A}{}^{J,\nu} |n_\alpha n_A; j_\alpha j_A m_\tau; JM\rangle\rangle^{(\nu)}. \quad (2.22)$$

The index ν on the particle-hole functions indicates that the particle continuum states obey the boundary conditions of the νth eigenchannel.

The normalizations of the wave function (2.22) and of (2.21) are different because (2.22) contains open as well as closed channels and the particle radial functions are normalized to unity in a sphere of radius a, while (2.21) contains only the open channels and the radial parts are normalized to unit flux. To obtain continuity of the nuclear wave function at $r=a$ we replace in (2.21) the V_c's by unnormalized coefficients $C_c^{J,\nu}$. By equating the thus modified expression (2.21) and the expression (2.22) at $r=a$ and integrating over all coordinates except r we obtain the matching condition

$$v_c{}^{-1/2} C_c{}^{J,\nu}[G_c(k_c a)\sin(\delta_J{}^{(\nu)}-\omega_c) +F_c(k_c a)\cos(\delta_J{}^{(\nu)}-\omega_c)]=\sum_n A_{nc}{}^{J,\nu} u_{nc}{}^{(\nu)}(a). \quad (2.23)$$

Finally, the amplitudes V of (2.21) can be obtained by normalization:

$$V_c{}^{J,\nu}=C_c{}^{J,\nu}/N_{J,\nu}, \quad (2.24)$$

$$N_{J,\nu}{}^2=\sum_c (C_c{}^{J,\nu})^2. \quad (2.25)$$

C. Formulas for the Reaction Cross Sections

The different possible particle cross sections are defined by an experimental situation in which an incoming wave exists only in one experimental channel and outgoing waves exist in all channels. The situation can be characterized by the quantum numbers $\alpha s u$. α indicates the target nucleus and the charge of the projectile, s is the channel spin, and μ its projection. Asymptotically, for large r, the properly normalized wave function which describes the process is given by

$$\Psi=v_\alpha{}^{-1/2} e^{ik_\alpha z_A}\Psi_{j_\alpha s_A}{}^{s\mu *}\varphi_\alpha +i\lambda_\alpha \sum_{\alpha' s' \mu'} v_{\alpha'}{}^{-1/2} Q_{\alpha' s' \mu';\alpha s \mu}(\theta,\varphi) r_A{}^{-1} e^{ik_{\alpha'} r_A} \times \Psi_{j_{\alpha'} s_{\alpha'}}{}^{s'\mu'}\varphi_{\alpha'}. \quad (2.26)$$

$\Psi^{s\mu}$ has been defined in (2.7) and φ_a in (2.9). By expanding the incident particle wave in terms of asymptotic eigenchannel functions, one obtains for the scattering amplitude

$$Q_{\alpha' s' \mu';\alpha s \mu}(\theta,\varphi)=\sum_J \sum_{ll'} \sum_{m'} i^{l-l'}\pi^{1/2} \times (2l+1)^{1/2}(ls0\mu|J\mu)(l's'm'\mu'|Jm'+\mu') \times[\delta_{\alpha\alpha'}\delta_{ss'}\delta_{ll'}-\tilde{S}_{\alpha' s' l';\alpha s l}{}^J] Y_{l'm'}{}^*(\theta,\varphi), \quad (2.27)$$

where the dependence of $\tilde{S}^J$ on the eigenchannel parameters $\delta^{(\nu)}$ and $V^{J,\nu}$ can be seen from (2.17) and (2.16). The partial cross section for the reaction $\alpha s \rightarrow \alpha' s'$ follows from

$$\frac{d\sigma_{\alpha' s';\alpha s}}{d\Omega}=\frac{\lambda_\alpha{}^2}{2s+1}\sum_{\mu\mu'}|Q_{\alpha' s' \mu';\alpha s \mu}(\theta,\varphi)|^2. \quad (2.28)$$

[16] E. Vogt, Rev. Mod. Phys. 34, 723 (1962).

Using the proper statistical weights, one obtains for a process where the channel spin is not observed

$$d\sigma_{\alpha'\alpha}=\sum_{s's}\frac{2s+1}{(2s_A+1)(2j_a+1)}d\sigma_{\alpha's';\alpha s}. \quad (2.29)$$

s_A denotes the spin of the scattered particle and j_a the nuclear spin of the target. Inserting (2.28), (2.27), (2.17), and (2.16) in (2.29) and expanding the angular distribution in terms of Legendre polynomials, we finally obtain

$$\frac{d\sigma_{\alpha'\alpha}}{d\Omega}=\frac{\lambda\!\!\!^{-}_{\alpha}{}^2}{(2s_A+1)(2j_a+1)}\sum_{L=0}^{L_{max}}\sum_{s's}B_L(\alpha's';\alpha s)\times P_L(\cos\theta), \quad (2.30)$$

where

$$\sum_{s's}B_L(\alpha's';\alpha s)=\sum_{J_1J_2}\sum_{\nu_1\nu_2}(2J_1+1)(2J_2+1)\times\sin\delta_{J_1}{}^{(\nu_1)}\sin\delta_{J_2}{}^{(\nu_2)}\cos(\delta_{J_1}{}^{(\nu_1)}-\delta_{J_2}{}^{(\nu_2)})\times\Theta_L(\alpha,J_1\nu_1,J_2\nu_2)\Theta_L(\alpha',J_1\nu_1,J_2\nu_2), \quad (2.31)$$

$$\Theta_L(\alpha,J_1\nu_1,J_2\nu_2)=(-)^{j_a-1/2}\sum_{l_1j_1}\sum_{l_2l_2}i^{L+l_1-l_2}\times[(2l_1+1)(2l_2+1)(2j_1+1)(2j_2+1)]^{1/2}\times(l_1l_200|L0)W(J_1J_2j_1j_2;Lj_a)\times W(l_1l_2j_1j_2;L\tfrac{1}{2})V_{\alpha l_1j_1}{}^{J_1,\nu_1}V_{\alpha l_2j_2}{}^{J_2,\nu_2}. \quad (2.32)$$

The sums over ν_1 and ν_2 go independently over all eigenvectors of the S matrix. Equation (2.30) gives the angular distribution for a process $\alpha\rightarrow\alpha'$, where α characterizes the charge of the particle as well as the charge and excitation of the residual nucleus. This formula gives the elastic scattering cross sections and the various particle-particle reaction cross sections. In (2.31) the eigenphases occur in the same manner as the scattering phase shifts do in (2.4).

By integrating (2.30) over the solid angle, one obtains

$$\sigma_{\alpha'\alpha}=\sum_J\frac{\pi\lambda\!\!\!^{-}_{\alpha}{}^2(2J+1)}{(2s_A+1)(2j_a+1)}\times\sum_{lj}\sum_{l'j'}|\delta_{\alpha\alpha'}\delta_{ll'}\delta_{jj'}-S_{\alpha'l'j';\alpha lj}{}^J|^2. \quad (2.33)$$

Summing over the final target states leads to the total cross section for bombarding an initial target state α:

$$\sigma_\alpha=\frac{4\pi\lambda\!\!\!^{-}_{\alpha}{}^2}{(2s_A+1)(2j_a+1)}\sum_{\alpha'}\sum_{ss'}B_0(\alpha's';\alpha s)$$

$$=\frac{2\pi\lambda\!\!\!^{-}_{\alpha}{}^2}{(2s_A+1)(2j_a+1)}\sum_J(2J+1)\times\sum_{lj}[1-\mathrm{Re}S_{\alpha lj;\,\alpha lj}{}^J]$$

$$=\frac{2\pi\lambda\!\!\!^{-}_{\alpha}{}^2}{(2s_A+1)(2j_a+1)}\sum_J(2J+1)\times\sum_{lj}[1-\sum_\nu(V_{\alpha lj}{}^{J,\nu})^2\cos2\delta_J{}^{(\nu)}]. \quad (2.34)$$

3. PHOTONUCLEAR CROSS SECTIONS

As already mentioned in the Introduction, the photon channels can be treated by perturbation methods. Thus photon emission and absorption processes are described as transitions between, say, the ground state of a nucleus and a particular eigenchannel state. A transition involving a linear combination of eigenchannel states, e.g., the process $O^{16}(\gamma,p_1)N^{15*}$, is then described by a suitable superposition of the matrix elements for these eigenchannels.

Thus, we want to compute

$$\sigma_\pm=(2\pi/\hbar)\rho_E(2\pi\hbar\omega e^2/c)|M|^2 \quad (3.1)$$

for the absorption cross section.[17] Here, the subscripts $\pm$ refer to the photon polarization and, specializing to electric dipole transitions,

$$M=(4\pi/3)^{1/2}\langle f|rY_{1\pm1}|i\rangle, \quad (3.2)$$

where the state $|f\rangle$ is, say, an eigenchannel state of the form (2.21). In (3.1) and (3.2) the density of the final states ρ_E and the normalization of the final-state wave function $|f\rangle$ must be defined together in a consistent manner. We do it by using the eigendifferential method of Weyl. According to that method a continuum state is made normalizable to unity by integration over a finite but small energy interval ΔE. We shall denote such a state by $|\tilde{f}\rangle$. Then the density of states is simply

$$\rho_E=1/\Delta E. \quad (3.3)$$

As long as ΔE is very small the radial wave function is modified only at very large radii. Thus the modification of the wave function needed for convergence of the normalization integral is confined to extremely large r, say to $r>b$, so that all calculations for the matrix elements and the diverse matchings to be discussed can be performed with the nonmodified form of the wave function.

In the asymptotic region, but before the Weyl modifications set in, the final-state wave function has the form

$$|\tilde{f}\rangle=|f\rangle=\tilde{N}^{-1}\sum_c v_c^{-1/2}V_c w_c(r)\tilde{\psi}_c, \quad r<b \quad (3.4)$$

[17] M. Danos, Photonuclear Physics Lectures, University of Maryland, 1961 (unpublished).

which, except for the normalization constant $\tilde{N}$, is an abbreviated version of (2.21).

For the Weyl function we introduce the notation

$$\tilde{w}_c(r)=W_c\int_E^{E+\Delta E} dE\, w_c(r). \tag{3.5}$$

Here the normalization constant W_c is chosen such that for the nonmodified region of the Weyl function there holds

$$\tilde{w}_c(r)=w_c(r) \quad \text{for} \quad r<b. \tag{3.6}$$

Then $|f\rangle$ goes over to $|\tilde{f}\rangle$ upon replacing w_c by $\tilde{w}_c$ in (3.4). The normalization condition for the wave function (3.4) thus becomes

$$1=\langle\tilde{f}|\tilde{f}\rangle=\tilde{N}^{-2}\sum_c v_c^{-1}(V_c)^2\langle\tilde{w}_c|\tilde{w}_c\rangle. \tag{3.7}$$

This completes the general formulation.

We now go over to the details. We begin with Eq. (3.5). In the region $r\approx b$ the function $w_c(r)$ has already the completely asymptotic form $w_c(r)=\sin(k_c r+\delta-\frac{1}{2}l\pi)/r$. The addition of the logarithmic Coulomb phase in the case of charged particles is of no importance in the present context. We therefore can do the matching (3.6) using this asymptotic form of $w_c(r)$. This then leads to the equation

$$W_c=M_{\rm red}/(\gamma\hbar^2k_c^2)=1/\Delta E. \tag{3.8}$$

Here $M_{\rm red}$ is the reduced mass, and we have used the abbreviation $\gamma=\Delta E M_{\rm red}/(\hbar^2k^2)$. It has the physical meaning of defining the energy interval of the integration in (3.5) in terms of the momentum variable, i.e., if the limits of the integration are k_1 and k_2, then $k_2=k_1(1+\gamma)$. With (3.8) we have for the normalization of the Weyl functions

$$\langle\tilde{w}_c|\tilde{w}_c\rangle=(\pi k\hbar^2/2M_{\rm red})(1/\Delta E). \tag{3.9}$$

Finally, we obtain for the over-all normalization constant

$$\tilde{N}^2=\tfrac{1}{2}\pi\hbar(1/\Delta E). \tag{3.10}$$

We now turn to the detailed form of the matrix element (3.2). Because of the normalization (3.6) the matrix element computed with the Weyl function $|\tilde{f}\rangle$ is the same as that computed with the unmodified function $|f\rangle$. We thus can insert (3.4) in (3.2), or more precisely, the equivalent inside solution (2.22) supplemented with the normalization constant $(\tilde{N}N_{J,\nu})^{-1}$. Here $N_{J,\nu}$ accounts for the different normalization of the eigenchannel functions for $r<a$ and $r>a$ and is given by (2.25).

This way we finally obtain for the total dipole absorption cross section

$$\sigma_\pm=4\pi^2(e^2/\hbar c)(\hbar\omega)\sum_\nu|M_\nu|^2, \tag{3.11}$$

where, using the wave function (2.22), the matrix element M_ν is given by

$$M_\nu=(4\pi/3)^{1/2}[\tfrac{1}{2}\pi\hbar\sum_c(C_c)^2]^{-1/2}\langle\Psi^{J,\nu}|rY_{1\pm1}|i\rangle. \tag{3.12}$$

We now turn to some examples of partial cross sections. We begin with the differential cross section of a process leading to a final state specified by α. Writing $\Psi_\alpha{}^\nu$ for a wave function (2.22) in which the summation over α has been omitted, and introducing the notation

$$\Psi_\alpha=\sum_\nu M_\nu\Psi_\alpha{}^\nu, \tag{3.13}$$

we have for the differential cross section

$$d\sigma_\alpha/d\Omega\propto\Psi_\alpha{}^*\Psi_\alpha=\sum_L\langle\Psi_\alpha|P_L|\Psi_\alpha\rangle P_L. \tag{3.14}$$

For the coefficients of the angular distribution we obtain

$$\begin{aligned}q\langle\Psi_\alpha|P_L|\Psi_\alpha\rangle=&\pi(e^2/\hbar c)(\hbar\omega)\sum_s\sum_{lj\nu}\sum_{l'j'\nu'}\cos(\delta_1{}^{(\nu)}-\delta_1{}^{(\nu')})\\&\times V_{\alpha lj}{}^{1,\nu}M_\nu V_{\alpha l'j'}{}^{1,\nu'}M_{\nu'}(-)^{(1/2)(l+l')}[3(2L+1)(2j+1)\\&\times(2j'+1)(2l+1)(2l'+1)]^{1/2}(ll'00|L0)\tfrac{1}{2}[1+(-)^L]\\&\times(L101|11)(2s+1)W(l'sL1;1l)W(j_a sjl;\tfrac{1}{2}1)\\&\times W(l'sj'j_a;1\tfrac{1}{2}).\end{aligned} \tag{3.15}$$

The constant q converts the angular distribution (3.14) into an absolute cross section. The summation over the channel spin s can be performed explicitly. This way the product of three Racah coefficients in (3.15) reduces to a product of two Racah coefficients. Integrating over the solid angle we have for the partial cross section

$$\begin{aligned}\int(d\sigma_\alpha/d\Omega)d\Omega&=4\pi q\langle\Psi_\alpha|P_0|\Psi_\alpha\rangle\\&=4\pi^2(e^2/\hbar c)(\hbar\omega)\sum_{lj}|\sum_\nu e^{i\delta_1{}^{(\nu)}}V_{\alpha lj}{}^{1,\nu}M_\nu|^2.\end{aligned} \tag{3.16}$$

4. SOLUTION OF THE NUCLEAR PROBLEM

A. Single-Particle Wave Functions

The radial single-particle wave functions $u_{nlj}(r)$ are obtained from an optical model, i.e., by solving the differential equation

$$\frac{d^2u_n}{dr^2}+\frac{2M_{\rm red}}{\hbar^2}\left(\epsilon_n-\frac{l(l+1)\hbar^2}{2M_{\rm red}r^2}-V(r)\right)u_n=0. \tag{4.1}$$

The potential $V(r)$ is taken to be real and of the Saxon-Woods type including a spin-orbit term and, in the case of protons, a Coulomb term. The charge distribution is assumed to be homogeneous so that

$$V(r)=V_c\left[e(r)-\gamma\left(\frac{\hbar}{2Mc}\right)^2(\mathbf{l}\cdot\boldsymbol{\sigma})\frac{1}{r}\frac{de(r)}{dr}\right]+V_{\rm Coul}, \tag{4.2}$$

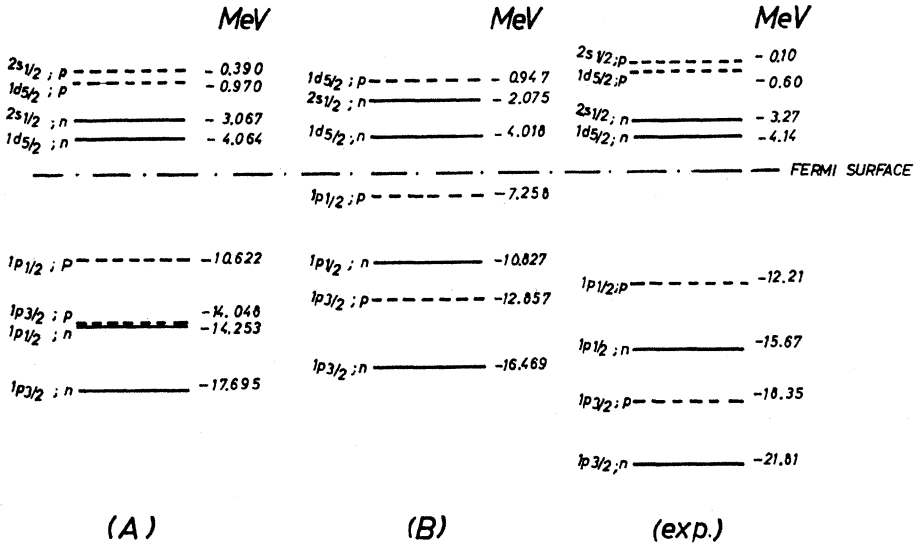

FIG. 1. Position of the bound proton and neutron states for the potentials A and B given in the text, compared with the experimental level scheme. Potential A yields a good fit to the experimental level scheme above the Fermi surface; potential B follows from neutron scattering.

$$V_{\text{Coul}}=(Ze^2/2R_0)[3-(r/R_0)^2], \quad \text{for} \quad r\leq R_0$$
$$=Ze^2/r, \quad \text{for} \quad r\geq R_0. \qquad (4.2')$$

R_0 denotes the radius and Z the charge of the residual nucleus, M is the particle mass, and γ is a constant. Further,

$$\rho(r)=[1+\exp\{(r-R_0)/t\}]^{-1}, \qquad (4.3)$$

where t is the surface thickness parameter of the Fermi distribution.

The wave functions of the O^{16} compound system were computed with two different sets of potential parameters,

$$R_0=3.15\text{ F},\ t=0.65\text{ F},\ V_c=-53\text{ MeV},\ \gamma=20, \qquad (4.4a)$$

$$R_0=3.15\text{ F},\ t=0.65\text{ F},\ V_c=-50\text{ MeV},\ \gamma=35. \qquad (4.4b)$$

These two sets of parameters have the following characteristics. Both sets yield the correct position of the first level above the Fermi surface, i.e., of the $1d_{5/2}$-neutron state (see Fig. 1). The set A reproduces the energies of the bound states, i.e., the s-d shell levels, reasonably well, including the $\mathbf{l}\cdot\mathbf{s}$ splitting, while the set B has the correct $\mathbf{l}\cdot\mathbf{s}$ splitting for the p shell and agrees with neutron scattering data.[18]

In the calculations we use for the particle energies directly those given by the optical model. However, the hole energies are taken from experiment as is customary in particle-hole calculations. This is essential in order to obtain the correct particle thresholds.

The boundary surface was placed at

$$a=12\text{ F}. \qquad (4.5)$$

In Fig. 2, the numerically obtained logarithmic derivative for $d_{3/2}$-neutron states (set B) at $r=a$ is plotted as a function of energy $\epsilon\geq 0$. This example illustrates the density of positive-energy states which arises when using the value (4.5) for the matching radius a. A fixed boundary condition can be represented by a horizontal line whose points of intersection with the cotangent-shaped curve determine the discrete particle energies for the states with different radial quantum numbers.

Suppressing the radial quantum numbers, there are 10 1-particle–1-hole configurations contributing to the 1^- compound states of O^{16} [14,15] which we take into account:

(1) $(d_{3/2}\bar{p}_{3/2})_n$, (2) $(d_{5/2}\bar{p}_{3/2})_n$, (3) $(s_{1/2}\bar{p}_{3/2})_n$,
(4) $(d_{3/2}\bar{p}_{1/2})_n$, (5) $(s_{1/2}\bar{p}_{1/2})_n$, (6) $(d_{3/2}\bar{p}_{3/2})_p$,
(7) $(d_{5/2}\bar{p}_{3/2})_p$, (8) $(s_{1/2}\bar{p}_{3/2})_p$, (9) $(d_{3/2}\bar{p}_{1/2})_p$,
(10) $(s_{1/2}\bar{p}_{1/2})_p$.

We shall use the above numbering of the channels throughout the rest of the paper. So, e.g., $c=6$ will refer to the $d_{3/2}\bar{p}_{3/2}$ proton channel.

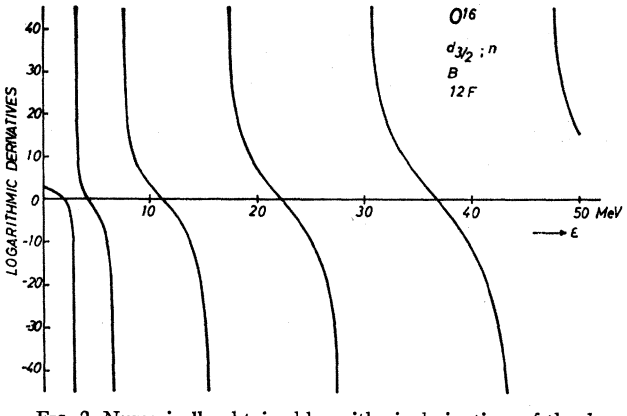

FIG. 2. Numerically obtained logarithmic derivatives of the $d_{3/2}$ radial wave functions for neutrons in O^{16} (potential B) at 12 F versus energy ϵ ($\epsilon\geq 0$).

[18] F. Bjorklund and S. Fernbach, Phys. Rev. **109**, 1295 (1958).

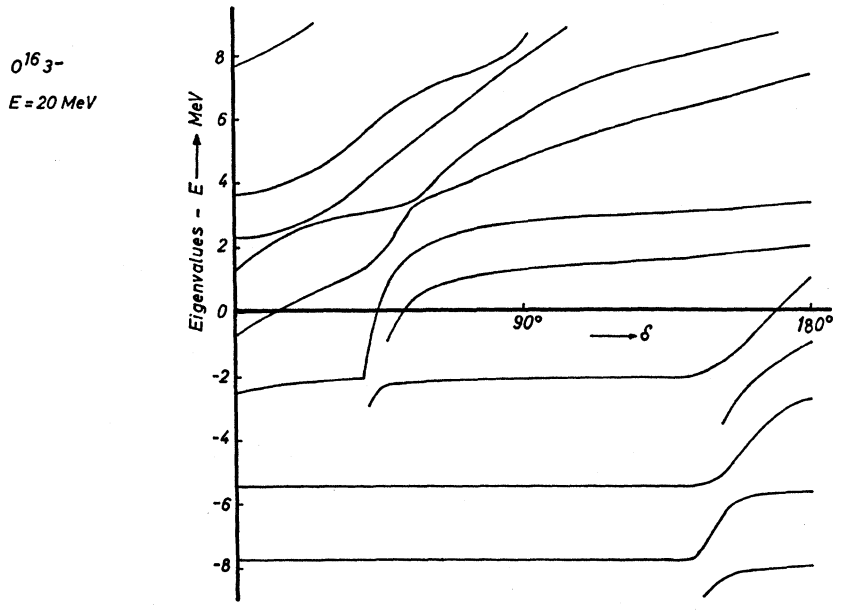

FIG. 3. Example of the behavior of the eigenvalues of the many-body Hamiltonian (more accurately $T_\lambda = E_\lambda - E$) as a function of the common phase δ which, together with the excitation energy E, determines the boundary conditions for the particle continuum states.

In the expansion of the nuclear wave functions (2.22), the particle states up to $\epsilon = 30$ MeV were included in the actual calculations.

The hole states were computed with boundary conditions at infinity, i.e., with exponentially decaying tails. The empirical thresholds for the various particle processes which have been used to fix the hole energies are listed in Table I.

B. Energy Matrix

The effective two-body force which is responsible for the residual interaction is assumed to be of the form

$$V(1,2) = V_0 J(r_{12})[a_0 + a_\sigma \boldsymbol{\sigma}(1)\cdot\boldsymbol{\sigma}(2) + a_\tau \boldsymbol{\tau}(1)\cdot\boldsymbol{\tau}(2) + a_{\sigma\tau}\boldsymbol{\sigma}(1)\cdot\boldsymbol{\sigma}(2)\boldsymbol{\tau}(1)\cdot\boldsymbol{\tau}(2)], \quad (4.6)$$

where $\boldsymbol{\tau}$ acts on the charge states of the particles or holes. In our actual computations we employed a contact force

$$J(r_{12}) = \delta(\mathbf{r}_1 - \mathbf{r}_2). \quad (4.7)$$

Then the matrix elements of the residual interaction can be cast into the form

$$V_{bB;aA} = (V_0/4\pi)(-)^{l_A+l_B}\hat{l}_a\hat{j}_A\hat{l}_b\hat{j}_B \times \hat{j}_a\hat{j}_A\hat{j}_b\hat{j}_B \sum_\lambda \sum_{S=0,1} (l_a l_A 00|\lambda 0)(l_b l_B 00|\lambda 0) \times G_S^{m_\tau A, m_\tau B}(2S+1) \begin{Bmatrix} l_a & \frac{1}{2} & j_a \\ l_A & \frac{1}{2} & j_A \\ \lambda & S & J \end{Bmatrix} \begin{Bmatrix} l_b & \frac{1}{2} & j_b \\ l_B & \frac{1}{2} & j_B \\ \lambda & S & J \end{Bmatrix} \times \int_0^\infty u_a u_A u_b u_B (1/r^2) dr, \quad (4.8)$$

TABLE I. Energies of the hole states.

Name of the residual nucleus	Configuration representing the residual nucleus	Type of particle	Q (MeV)
N^{15}	$\tilde{p}_{1/2}$	p	12.21
O^{15}	$\tilde{p}_{1/2}$	n	15.67
N^{15}	$\tilde{p}_{3/2}$	p	18.35
O^{15}	$\tilde{p}_{3/2}$	n	21.81

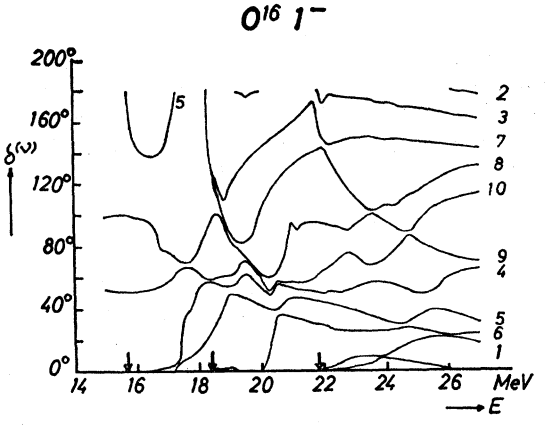

FIG. 4. Energy dependence of the eigenphases $\delta^{(\nu)}$ of the 1^- compound system. The parameter choice is that of potential B and a zero-range force with a strength of -1000 MeV F³. This combination is referred to as set III below. The numbers on the curves label the channels presumed dominant close to the thresholds. The enumeration is explained in the text. The positions of the thresholds are marked by arrows.

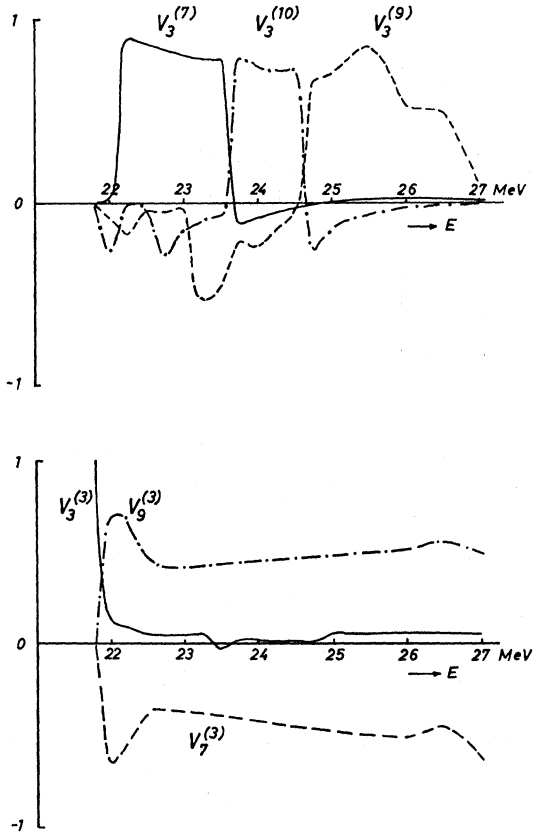

FIG. 5. Examples of the behavior of the amplitudes $V_c^{(\nu)}$ as a function of the energy.

where the exchange terms are

$$G_0^{m_\tau,m_\tau'}=(2-\delta_{m_\tau,m_\tau'})a_0-3\delta_{m_\tau,m_\tau'}a_\tau -3\delta_{m_\tau,m_\tau'}a_\sigma-3(2-\delta_{m_\tau,m_\tau'})a_{\sigma\tau}, \quad (4.9)$$

$$G_1^{m_\tau,m_\tau'}=-\delta_{m_\tau,m_\tau'}a_0-(2-\delta_{m_\tau,m_\tau'})a_\tau +(2+\delta_{m_\tau,m_\tau'})a_\sigma+(4-5\delta_{m_\tau,m_\tau'})a_{\sigma\tau},$$

and $\hat{x}=(2x+1)^{1/2}$. The complete energy matrix is thus given by

$$H_{bB;aA}=\delta_{ab}\delta_{AB}[\epsilon_A-\epsilon_a]+V_{bB;aA}, \quad (4.10)$$

where the ϵ's are the independent particle energies discussed in the last section. The exchange mixture in (4.6) is taken to be of the Meshkov-Soper type[19];

$$a_0=0.865, \quad a_\sigma=0.135, \quad a_\tau=a_{\sigma\tau}=0. \quad (4.11)$$

For the strength of the zero-range force, two values were employed:

$$V_0=-650 \text{ MeV F}^3 \quad (4.12a)$$

and

$$V_0=-1000 \text{ MeV F}^3. \quad (4.12b)$$

[19] S. Meshkov and C. W. Ufford, Phys. Rev. **101**, 734 (1956).

The first value agrees with the standard model of Ref. 6. Since the oscillator well which is equivalent to our Saxon-Woods potential has a spacing $\hbar\omega=16$ MeV (length parameter $\beta=1.61$ F), the value (4.12a) is close to the one used in particle-hole calculations for O^{15} ($V_0/4\pi\beta^3=-11.46$ MeV).[20] The second value (4.12b) has been tried in order to obtain better agreement with experiment.

C. Search for Eigenphases

The nuclear eigenvalue problem is completely specified if the asymptotic wave numbers k_c and the common phase shift δ are given specific values. Then the boundary conditions for the single-particle functions of

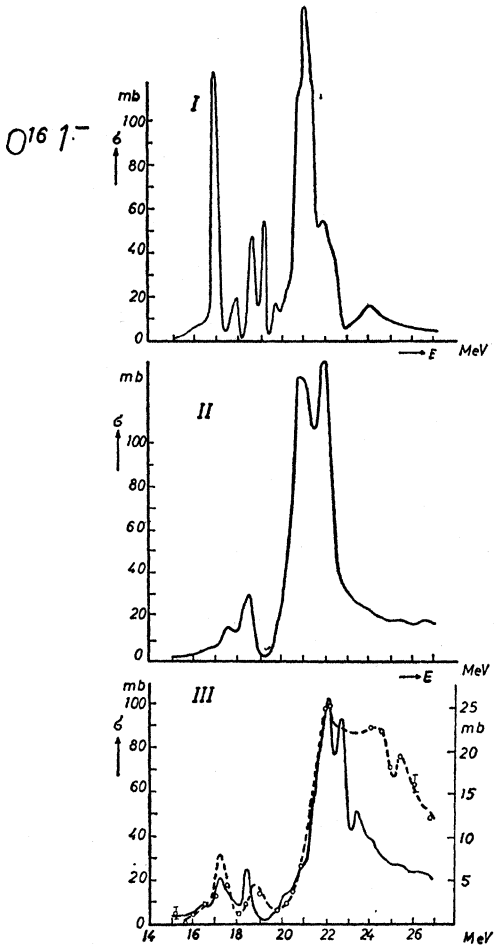

FIG. 6. The total photonuclear cross section of O^{16} for the three different parameter sets defined in the text, compared with the total γ-absorption data of Wyckoff *et al.* (Ref. 22). The scale on the right-hand side of the lowest figure is taken from Ref. 22. Here, and in the following figures, the computations for set I have been done only above 19 MeV.

[20] O. Bohigas, in *Proceedings of the International Conference on Nuclear Physics, Gatlinburg, Tennessee, 1966* (Academic Press Inc., New York, 1967).

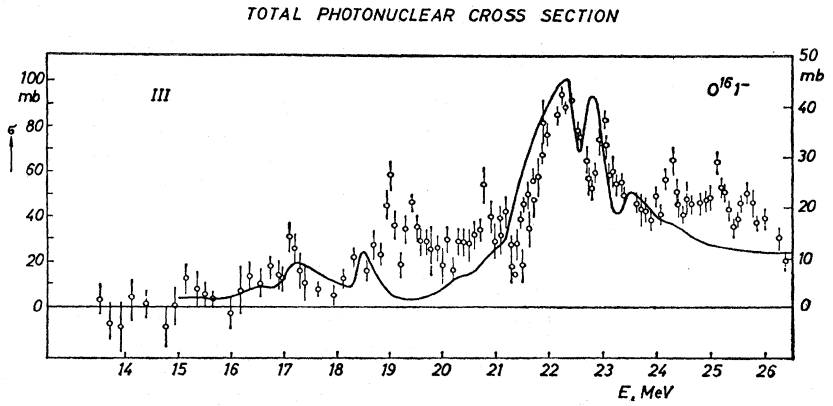

FIG. 7. Comparison of the theoretical total photon absorption cross section (set III) and the measured data of Burgov *et al.* (Ref. 23). The experimental scale is on the right.

the various channels can be calculated and the corresponding particle-hole functions can be constructed. For the states appearing only in closed channels arbitrary boundary conditions can be employed.

At a given energy E of the compound system the wave numbers k_c in the different experimental channels c are given by

$$E=(\hbar^2/2M_{\text{red}})k_c^2+Q_c, \tag{4.13}$$

where Q_c is the threshold energy. Thus, given an energy E the energy matrix (4.10) can be computed for any phase δ. By diagonalizing these matrices one then generates the eigenvalues E_λ and the eigenvectors A (2.22) as functions of δ. Finally, the eigenphases $\delta^{(\nu)}$ are found as the solutions of the transcendental consistency equation

$$T_\lambda(\delta)=E_\lambda(\delta)-E=0. \tag{4.14}$$

Figure 3 gives an example for the behavior of T_λ as a function of the phase δ. We show a plot for the 3^- states in O^{16} since they are less involved than the 1^- states. E is equal to 20 MeV at which energy four of the six 3^- channels are open. It is obvious from the figure that there are four eigenphases.

The "kinematics" of the plot (Fig. 3) is the following. Since the logarithmic derivative is a periodic function of δ with a period π, the topology of the plot is that of a cylinder. The eigenvalue curves are thus interlaced helices which do not cross as they "wind their way up." This is simply a consequence of Wigner's no-crossing theorem: At any fixed value of δ the eigenvalues of the Hamiltonian with an overwhelming probability are nondegenerate. Therefore, a no-crossing theorem holds also for the eigenphases with the same kind of validity as for the eigenvalues of any Hamiltonian. The number of the eigenvalue lines equals the number of open channels, as can be seen by tracing each line "backwards." This is most transparent before switching on the residual interactions. Then each channel consists of a particle in the continuum together with an unperturbed residual nucleus in some discrete state. The energy of such a system then consists of a fixed energy of the hole state plus the energy of the free particle, which can be read off a plot of the kind of Fig. 2 as a function of the logarithmic derivative. Each open channel thus disappears at a particular phase shift. Switching on the residual interaction only shifts the energies somewhat and removes the level crossings.

The energy dependence of the eigenphases of the 1^- compound system of O^{16} is shown in Fig. 4. The parameters here are those of (4.4b) and (4.12b). The step width was about 0.25 MeV for the greatest part of the displayed energy range. The numbers on the curves indicate the channel which presumably is predominant near the respective thresholds and they correspond to

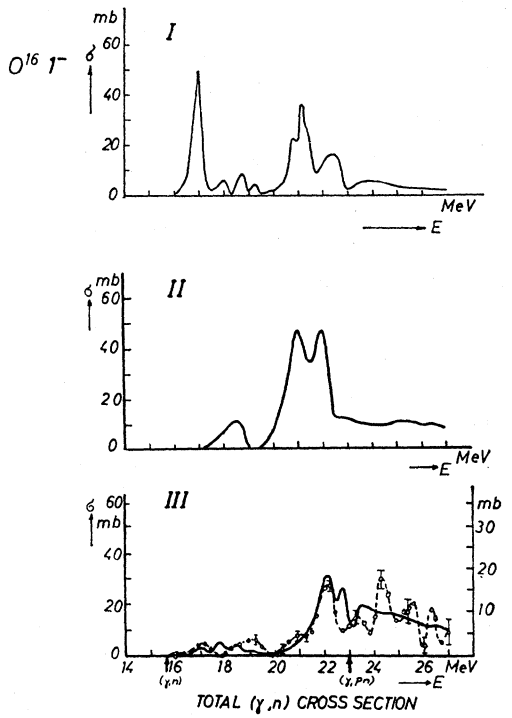

FIG. 8. The total (γ,n) cross section. The arrangement of the figure is the same as in Fig. 5. The experimental curve gives the $(\gamma,\Sigma n)$ data of Hayward and Stovall (Ref. 24). The (γ,pn) threshold is indicated.

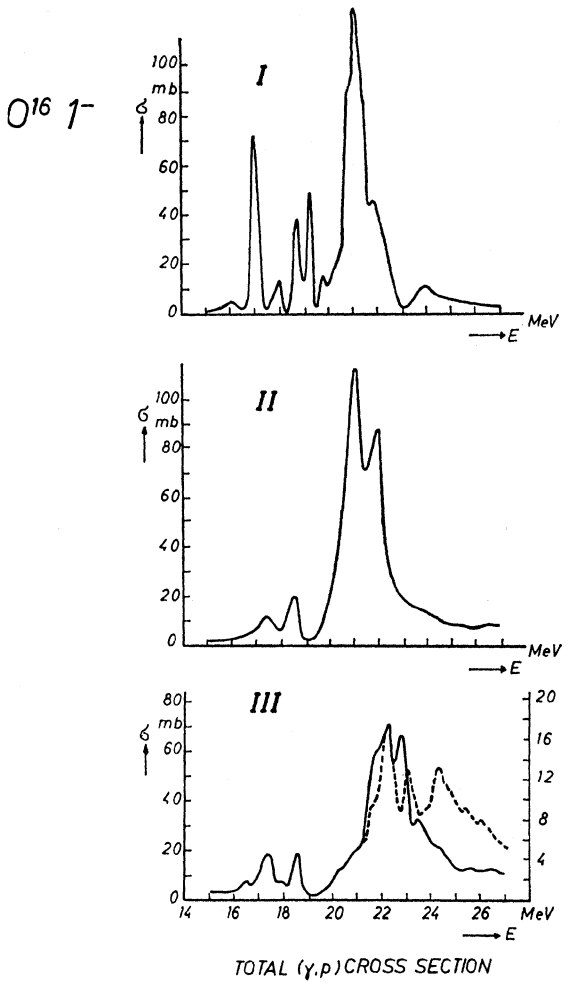

FIG. 9. Total (γ,p) cross section. The experimental curve is due to Morrison [R. C. Morrison, Yale University, thesis, 1965 (unpublished); also see Ref. 6].

the enumeration introduced in Sec. 4 A. The threshold energies are marked by arrows.

In the numerical search procedure the δ interval from 0° to 180° was repeatedly divided into halves up to an interval length of about 1.4°. Since it is easy to determine how many zeros of T_λ are contained within some δ interval, empty halves could be skipped. Finally the eigenphases were determined by interpolation within the relevant 1.4° intervals. The interpolation was carried out such that the corresponding values of $|T_\lambda|$ are smaller than 1 keV. This accuracy exceeds by about a factor of 10 the accuracy of the single-particle continuum energies which were taken from an interpolation formula.

The accuracy of the eigenchannel method depends on two parameters. The first is the magnitude of the function space. Its influence on the accuracy is here the same as in any shell-model calculations. It was found for the present calculation that a reduction of the function space by using three instead of four radial functions in each channel caused on the average a decrease of the eigenphases by 0.9°. The second parameter is the matching radius. This parameter determines the channel orthogonality and also the orthogonality of the wave functions used to obtain the inside solution. As can be seen by considering the character of the radial functions, orthogonality in the inside region between a bound state computed with boundary conditions at infinity and a continuum state is most difficult to fulfill near threshold; there the matching radius would have to be chosen larger than at other energies in order to achieve the same degree of orthogonality. In any case, it was found that decreasing the matching radius a from 12 to 11 F caused an average increase of the eigenphases by 0.3°.

A further test of the accuracy of our calculations is provided by the scalar products

$$\Delta_{\nu\nu'}=\sum_c V_c^{J,\nu}V_c^{J,\nu'},$$

which should be zero for $\nu\neq\nu'$. In the present case their magnitude turned out to be 0.03 or less on the average except for small regions immediately above thresholds where they sometimes were considerably larger.

The eigenvectors $V^{J,\nu}$ of the S matrix are obtained simultaneously with the eigenphases by making use of the continuity of the nuclear wave function at $r=a$ [see (2.23), (2.24), and (2.25)]. They are smooth but

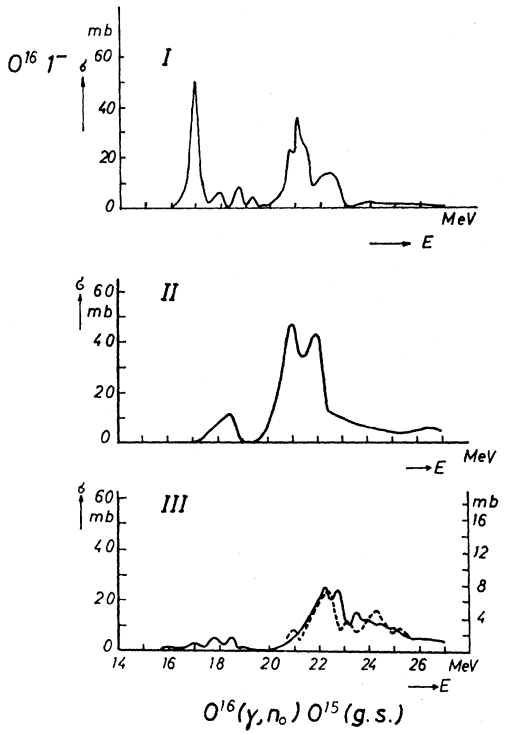

FIG. 10. The partial cross section of the photoneutron reaction leading to the ground state of O^{15}. The experimental curve is due to J. T. Caldwell *et al.*, Phys. Rev. Letters **15**, 176 (1965).

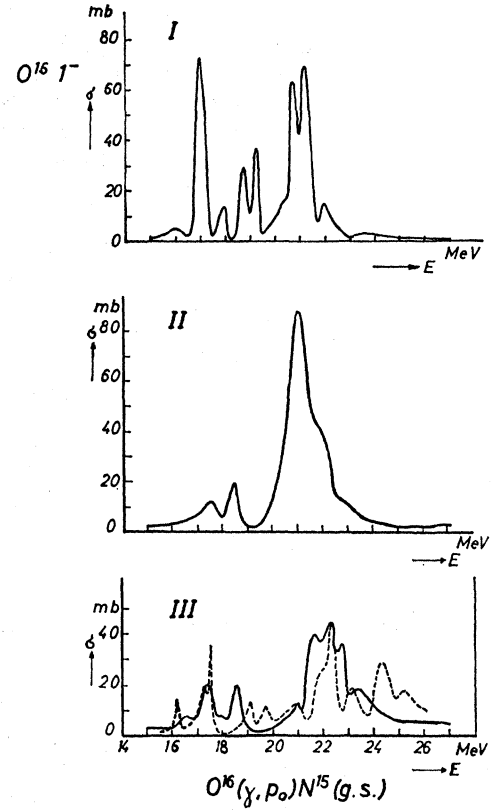

FIG. 11. The partial cross section of the photoproton reaction leading to the ground state of N^{15}. The experimental curve shows the relative yield at 90° obtained by N. W. Tanner *et al.*, Nucl. Phys. **52**, 45 (1964).

complicated functions of the energy E and it seems not to be worthwhile to exhibit them in detail. We give, however, some typical examples. In Table II are listed the eigenvectors of the S matrix. The excitation energy is 18.25 MeV, i.e., just below the threshold of the channels involving the $p_{3/2}$ proton hole state, and the parameter choice is that of (4.4b) and (4.12b). At this energy four of the 10 1^- channels are open. The scalar products $\Delta_{\nu\nu'}$ in decreasing order are 0.039, −0.014, 0.010, 0.004, etc.

The effect of the noncrossing theorem is illustrated in the top part of Fig. 5, taking as an example the channel $(s_{1/2}\tilde{p}_{3/2})_n$, i.e., the channel $c=3$. As can be seen in Fig. 4, this is the clearest case of an almost undistorted eigenstate, which goes against the general trend of the other eigenvalues and consequently has a series of crossings. Figure 5 shows that this state maintains a high degree of purity in between the crossings and "switches over" in a rather small energy interval. The bottom part of Fig. 5 demonstrates how the eigenchannel $\nu=3$ "loses its identity." After the first crossover, which here accidentally is very close to the threshold, the configuration $c=3$ switches over to the eigenchannel $\nu=7$ (top part of Fig. 3) while the eigenchannel $\nu=3$ becomes a mixture of several configurations, the largest of which are plotted in the figure.

As is evident, on the whole the energy dependence of all quantities is rather smooth. No violent fluctuations are apparent, in particular around the giant resonance peaks, i.e., around 22–23 MeV.

TABLE II. Eigenstates of the S matrix for the 1^- at 18.25 MeV (4 open channels).

ν / $\delta^{(\nu)}$	1 20.29°	2 57.99°	3 59.90°	4 90.00°
$c=$ 4	−0.9873	−0.0286	0.0205	0.1517
5	0.0084	0.4943	0.8878	−0.0284
9	0.1577	−0.0508	0.0477	0.9860
10	−0.0163	0.8674	−0.4573	0.0624

5. RESULTS AND DISCUSSION

Results for three different sets of parameters shall be compared with experiment:

(I) Spin-orbit force which gives the correct splitting of the d shell ($\gamma=20$) and usual strength of the contact force (−650 MeV F^3)—(4.4a) and (4.12a),

(II) Spin-orbit force which gives the correct splitting of the p shell ($\gamma=35$) and usual strength of the contact force (−650 MeV F^3)—(4.4b) and (4.12a),

(III) Spin-orbit force which gives the correct splitting of the p shell ($\gamma=35$) and a strong contact force (−1000 MeV F^3)—(4.4b) and (4.12b).

To begin with we shall consider the photodisintegration processes. We will plot the experimental cross sections only on the figures corresponding to set III which seem to be most consistent with the experimental results. For sets III and I the calculation was done in 0.25-MeV steps, for set II we have employed 0.5-MeV steps.

The absolute magnitude of the theoretical γ-absorption cross section integrated to 27 MeV turns out to be

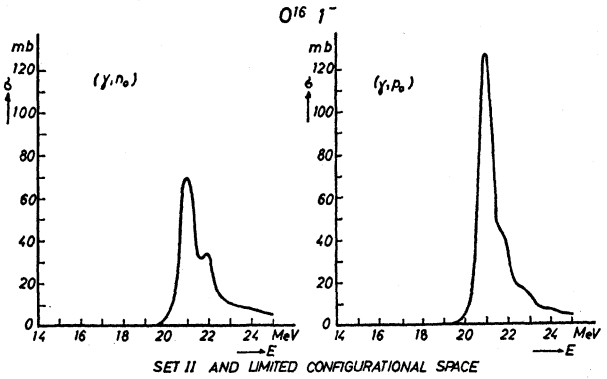

FIG. 12. This figure corresponds to Figs. 10 (II) and 11 (II), respectively. The only difference is that the configurational space was limited to the $(d_{5/2}\tilde{p}_{3/2})$ and $(d_{3/2}\tilde{p}_{1/2})$ neutron and proton configuration which predominate in the main peak. The similarities with Figs. 10 (II) and 11 (II) will be noticed.

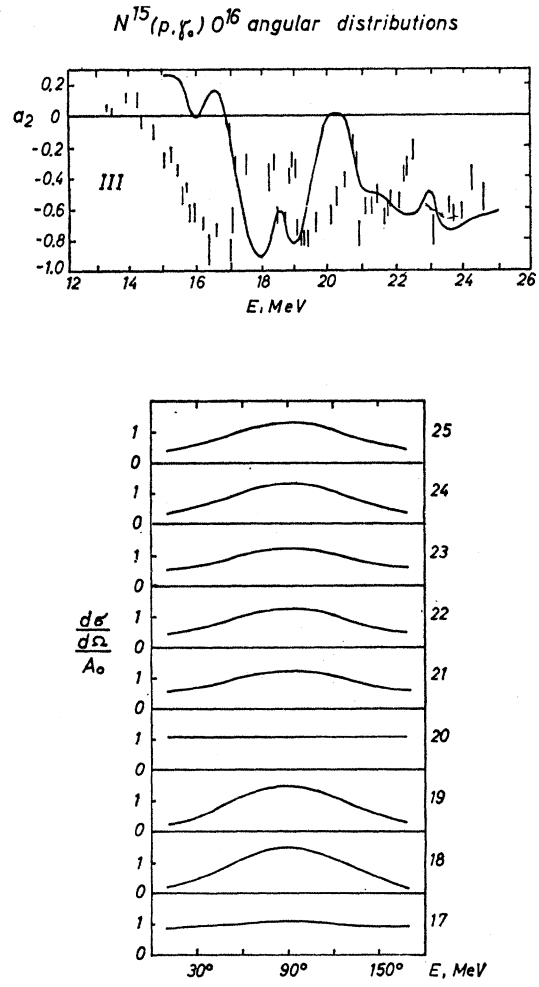

FIG. 13. Comparison of theory (set III) and experiment for the coefficients a_2 in a Legendre-polynomial expansion of the angular distribution of γ rays in the reaction $N^{15}(p,\gamma_0)O^{16}$ assuming pure dipole radiation, i.e., $d\sigma(p,\gamma_0)/d\Omega \propto 1+a_2P_2(\cos\theta)$. The data were obtained from Earle *et al.* (Ref. 25).

about $2\frac{1}{2}$ times as large as the experimental value.[21] Considering the height of the main peak the enhancement factor varies between 2 and 5.

Figure 6 gives the total dipole absorption cross sections for the parameter sets I–III. In case I the main peak occurs 1 MeV too low. It has a shoulder on the high-energy side. There is a second well-developed peak at 24 MeV. The ratio of the two peaks is 8, whereas the experimental ratio is 1.3.

In case II the main peak is still at the same position as in case I but its shoulder has developed into a separate peak. Both these peaks in II result from a $(d_{5/2}\tilde{p}_{3/2})$ configuration with a strong $(d_{3/2}\tilde{p}_{1/2})$ admixture. Still, the influence of the other configurations is very important as will be demonstrated below. The main contribution in Fig. 6 (II) at 24 MeV results, however, from a $(d_{3/2}\tilde{p}_{3/2})$ configuration with $(s_{1/2}\tilde{p}_{3/2})$ admixture. Instead of the small peak seen in case I now one observes a broad shoulder. In this respect our result resembles that of Ref. 6.

In case III, finally, the main peak occurs at the right position. The experimental curve is that of Wyckoff *et al.*[22] The main features are reproduced by the theoretical curve; it should, however, be kept in mind that the energy resolution of this particular measurement was not too high. The same theoretical curve has been plotted in Fig. 7 together with the experimental results of Burgov *et al.*[23] This figure seems to be even more convincing. The theoretical ratio of the 22.2-MeV peak to the peak at 23.4 MeV is 1.9, i.e., it is much closer to the experimental ratio 1.3 for the heights of the 22.2- and 24.3-MeV peaks than the corresponding values from Refs. 14, 4 or 10. Furthermore, our results seem to indicate that some fraction of the dipole strength of the experimental 23.3-MeV peak can already be explained by 1-particle–1-hole continuum calculations.

Figure 8 gives the results for the (γ,n) process. It is seen that the theoretical main peak is always split into two peaks and there is a small peak between 23 and 24 MeV. The experimental data are from Hayward and Stovall.[24]

In Figs. 9–11 we have plotted (γ,p), (γ,n_0), and (γ,p_0) cross sections, respectively. It should be mentioned that the ratios of the (γ,p) to (γ,n) cross sections (integrated from 15 to 27 MeV) turn out to be 2.5, 1.9, and 2.1 in the three different cases I–III.

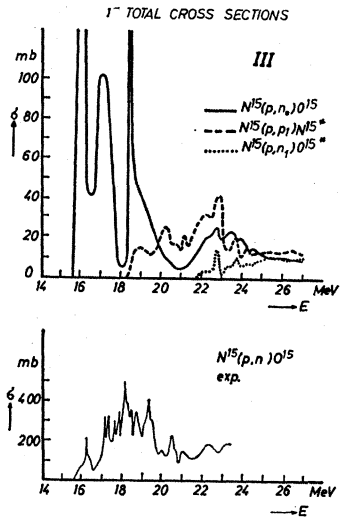

FIG. 14. Predicted inelastic particle-particle cross sections in the channels with $J^\pi=1^-$ for protons incident of N^{15}. The lower part of the figure shows the experimental (p,n) cross section of Barnett and Thomas (Ref. 26).

[21] R. L. Bramblett, J. T. Caldwell, R. R. Harvey, and S. C. Fultz, Phys. Rev. 133, B869 (1964).

[22] J. M. Wyckoff, B. Ziegler, H. W. Koch, and R. Uhlig, Phys. Rev. 137, B576 (1965).

[23] N. A. Burgov, G. V. Danilyan, B. S. Dolbilkin, L. E. Lazareva, and F. A. Nikolaev, Zh. Eksperim. i Teor. Fiz. 43, 70 (1962) [English transl.: Soviet Phys.—JETP 16, 50 (1963)].

[24] E. Hayward and T. Stovall, Nucl. Phys. 69, 241 (1965).

As already mentioned, the configurations $(d_{5/2}\tilde{p}_{3/2})$ and $(d_{3/2}\tilde{p}_{1/2})$constitute the major part of the wave function. To illustrate the effect of the minor components, we show Fig. 12 where they have been omitted from the calculation. Evidently they redistribute the dipole strength between the different peaks without affecting their positions.

In Fig. 13 we compare the a_2 coefficients of the angular distribution $1+a_2P_2(\cos\theta)$ for $^{15}\mathrm{N}(p,\gamma_0)^{16}\mathrm{O}$ with experiment[25] without, however, correcting for admixture of quadrupole radiation. The deviation from the experimental results is similar as in Ref. 6.

Because of the large difference in threshold energies the complete treatment has been carried through treating protons and neutrons as different particles, i.e., the isospin formalism was not employed. It is of interest to note that in the giant resonance region, i.e., at 21–23 MeV, the main configurations in the eigenchannels with large dipole moments are very pure $T=1$ states; the $T=0$ admixture is there only of the order 5–20% in *amplitude*.

For completeness we show the proton-induced particle cross sections for the parameter set III in Fig. 14 together with an experimental curve for the $^{15}\mathrm{N}(p,n)^{15}\mathrm{O}$ reaction.[26] It should be kept in mind that many angular momenta of the compound system contribute to the experimental cross section while the theoretical curve contains only the contributions of the 1^- states. It is thus not surprising that the experimental cross section shows more structure than the theoretical curve. Our result accounts only for one peak each in the regions around 16, 17, and 18.4 MeV, respectively. Taking an over-all look at the several cross-section curves one notices that they cannot really be represented by a superposition of Lorentz lines. This is in fact gratifying. As it has been known to electrical engineers for a long time,[27] and as nuclear physicists are beginning to realize, there exists an essential difference between the regions where only one channel is open and where more than one channel is open. In the language of electrical engineering, the former region corresponds to a two-pole network built of essentially lossless components: The only damping is provided by photon emission, which in that energy region is usually very small. Such networks can have only resonances. On the other hand, at the opening of a second channel the system becomes the analog of a four-pole network. The output load, i.e., the second continuum, now adds additional damping to the network and as a consequence it becomes a filter, which in addition to simple resonances may exhibit a more complicated behavior, such as pass-bands and stop-bands of varying shapes (not every filter transmission curve is nicely symmetric, as anyone who has tried to tune up an IF-strip can testify). Since the present case has up to 10 open channels it corresponds to a 20-pole network and quite complicated cross-section shapes have to be expected.

Finally, we may state that our results show more structure than those of other continuum calculations.[4,6] This is the main difference between these calculations and ours. Some of the fine structure may simply be calculational "noise." Recall, for example, that the orthogonality of the computed eigenchannels was not complete but of the order of 1% (Sec. 4 A). Since the cross sections result from coherent superpositions of all the eigenchannels, clearly, artificial fluctuations in the cross sections are to be expected. On the other hand, the broad features, e.g., the splitting of the main peak, should not be affected by these uncertainties. Indeed, our curves reflect a large part of the experimentally observed structure, in particular in the total photon absorption cross section. Undoubtedly the 2-particle–2-hole and higher configurations, as well as ground-state impurities, are indispensable for the explanation of the remaining discrepancies between theory and experiment, both with respect to fine structure and absolute magnitude of the cross sections. Anyway, it seems to us that one can account for the main features, and perhaps even for some of the fine structure already in the 1-particle–1-hole approximation, simply by the choice of the model parameters and by a careful treatment of the continuum. A calculation with inclusion of more complex configurations in the nuclear wave function is in progress. Furthermore, the influence of quadrupole radiation will also be tested.

ACKNOWLEDGMENTS

We are grateful to R. Lemmer for some useful comments. Special thanks are extended to E. G. Fuller for his many critical discussions.

[25] E. D. Earle, N. W. Tanner, and G. C. Thomas, in *Comptes Rendus du Congres' International de Physique Nucleaire, II*, edited by P. Gungenberger (Centre National de Recherche Scientifique, Paris, 1964), p. 385.

[26] A. R. Barnett and G. C. Thomas, in *Comptes Rendus Congres' International de Physique Nucleaire, II*, edited by P. Gungenberger (Centre National de Recherche Scientifique, Paris, 1964), p. 387.

[27] See, for example, W. L. Everitt, *Communication Engineering* (McGraw-Hill Book Co., New York, 1932).